OPEN ACCESS

University of Dundee

University of Dundee

Cryogenic surface resistance of copper

Calatroni, Sergio; Arzeo, Marco; Aull, Sarah; Himmerlich, Marcel; Costa Pinto, Pedro; Vollenberg, Wilhelmus

Cryogenic surface resistance of copper: Investigation of the impact of surface treatments for secondary electron yield reduction

Sergio Calatroni,[*] Marco Arzeo, Sarah Aull, Marcel Himmerlich, Pedro Costa Pinto,
Wilhelmus Vollenberg, Beniamino Di Girolamo, Paul Cruikshank, and Paolo Chiggiato
CERN, CH-1211 Geneva 23, Switzerland

David Bajek, Stefan Wackerow, and Amin Abdolvand
School of Science and Engineering, University of Dundee, Dundee DD1 4HN, Scotland, United Kingdom

The surface resistance of copper samples with an amorphous carbon (a-C) coating or with laser surface structuring, the surface treatments of choice for electron cloud suppression in critical cryogenic sectors of the high-luminosity upgrade of the Large Hadron Collider (HL-LHC), has been measured for the first time at a cryogenic temperature using the quadrupole resonator at CERN. Three different frequencies of relevance for evaluating beam impedance effects, namely, 400, 800, and 1200 MHz, have been investigated. No significant increase in surface resistance is observed for the a-C coating, compared to plain copper. In the case of laser structuring, the surface resistance depends on the direction of the surface currents relative to the laser-engraved groove pattern. The increase is minimal for parallel patterns, but in the perpendicular case the surface resistance increases considerably. Radio frequency (rf) heating from wake losses would then also increase in the HL-LHC case; however, the reduction in the power deposited onto the cold surfaces thanks to electron cloud suppression would still outweigh this effect.

I. INTRODUCTION

Electron cloud (e-cloud) mitigation is an essential requirement in proton circular accelerators for guaranteeing beam stability at a high intensity [1,2]. Currently in the Large Hadron Collider (LHC) at CERN [3], this is achieved thanks to the activated non-evaporable getter coating in the room-temperature sections, which provides a secondary electron yield (SEY) of the beam-facing surfaces that is lower than the electron multiplication threshold, thus effectively suppressing e-cloud phenomena. In the cryogenic sections, e-cloud mitigation is instead obtained through beam scrubbing of the copper surfaces of the beam screens. For the high-luminosity upgrade of the LHC (HL-LHC), new *ad hoc* surface treatments are envisaged on selected components, in particular, on the beam screens of the inner triplet magnets focusing the beam in the four LHC interaction regions. The main focus in this case is the reduction of the heat load on the cryogenic system, due to the higher power deposited onto cold

surfaces by the e-cloud if no proper mitigation strategy is implemented [4,5], as a result of the modified beam parameters, and due to the higher rate of collision debris.

Amorphous carbon (a-C) coatings [6] have been extensively validated and applied to the Super Proton Synchrotron (SPS) accelerator at CERN and are the baseline surface treatment selected for the HL-LHC. These will be applied through a combination of *ex situ* and *in situ* coatings, either for the new focusing magnets in the high-luminosity interaction regions (IR1 and IR5) or for retrofitting of the existing ones in the low-luminosity interaction regions (IR2 and IR8) [7]. Laser-engineered surface structures (LESS) [8,9] produced on the copper surfaces facing the beam are also being considered as a possible option to reduce the SEY, due to their potential for *in situ* implementation [10], mandatory for retrofitting. Both these surface treatments have been tested and validated on 2.2-m-long beam screens installed in the cold bore experiment (COLDEX) facility at the CERN SPS [11,12], showing, in particular, their robustness after several thermal cycles from room to cryogenic temperature.

These treatments may, however, modify the copper surface resistance, thus affecting beam-induced rf heating due to wake losses, of particular relevance for the HL-LHC cryogenic components. Theoretical estimates indicate that, due to their high electrical resistivity and very small thickness compared to the calculated skin depth, a-C coatings should

have a negligible effect on the local power dissipation [13]. LESS, however, due to the peculiar production technique relying upon repetitive laser beam scanning in a linear pattern, might have a pronounced effect depending on the relative orientation of the scan lines with respect to the rf surface currents, on the depth of the groves produced, and, more generally, on the overall topography [14].

A direct evaluation of the impact of either treatment on the surface resistance has been attempted at the COLDEX facility [11,12]. The experiments carried out during several dedicated machine development runs confirmed full suppression of the e-cloud but were not able to discriminate any wake-induced heating, due to the limited sensitivity of the apparatus. Thus, a possible impact on the HL-LHC could not be excluded.

Independent measurements of laser-structured surfaces at 7.8 GHz and room temperature have indeed shown that the surface resistance might be strongly modified [15], although for a different set of laser-treatment parameters than those discussed here.

The critical role of these surface treatments as potential e-cloud mitigation in the HL-LHC motivates further experimental validation of the theoretical estimates. The HL-LHC beam power spectrum [16] spans a range from very low frequencies up to about 1 GHz, with the amplitude decreasing rapidly above this frequency. Therefore, validation must be conducted within this frequency range and necessarily at a cryogenic temperature, because of the temperature dependence of the electrical resistivity and, thus, of the skin depth.

In this paper, we report on the measurement of the surface resistance of both a-C-coated and LESS-treated copper using the superconducting quadrupole resonator (QPR) [17,18]. We first describe the measurement system and the sample preparation, followed by the experimental results and their possible implications for the HL-LHC.

II. EXPERIMENTAL SETUPS

A. The quadrupole resonator

The QPR consists of four bulk niobium hollow rods (2 mm thick and 16 mm in diameter), which act as a $\lambda/2$ transmission line resonator, cooled by an internal liquid helium flow. At their bottom end, the rods are closed in pairs by a 25-mm-radius half ring [see the schematics in Fig. 1(a)]. Right below the two half rings, at a nominal distance of 1 mm, the top face of the sample disk (75 mm diameter) is placed. The four rods are enclosed in a screening cylinder, directly cooled by a liquid helium bath, formed by two bulk niobium cans (2 mm thick and 210 mm in diameter). The cans are copper brazed to stainless steel flanges, used to seal the cavity at the middle. Such a design makes the cavity easy to open for ultrapure water rinsing, in order to remove dust contamination which might give rise to electron field emission. The sample with its support is inserted in a tubular aperture, of 4 mm wider diameter, closing the cavity at the bottom. Images of the whole QPR and of a copper sample with its support are shown in Fig. 1(b). The sample support is a hollow niobium cylinder,
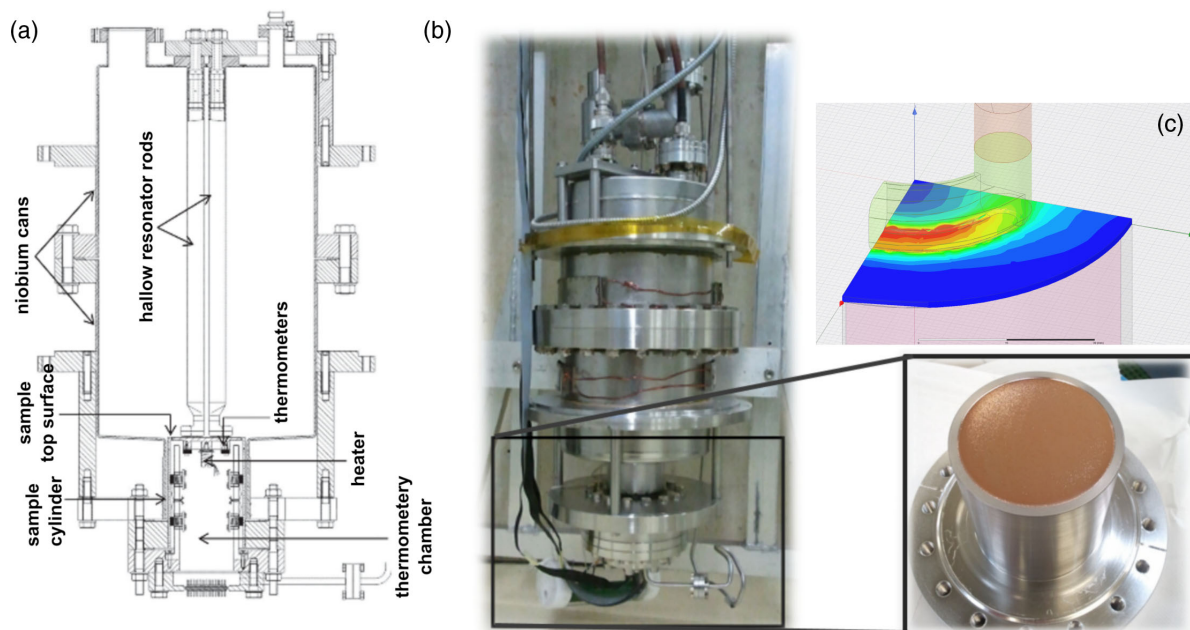
FIG. 1. The quadrupole resonator at CERN. (a) Schematic cross-section drawing, indicating the main parts: resonator rods, thermometers, heater, sample parts, and cavity cans [18]. (b) Photo of the quadrupole resonator at CERN and of a bare copper sample. (c) rf magnetic field pattern on a quarter of the sample surface for the 400 MHz quadrupole mode from numerical simulations. Red corresponds to the highest field, and blue to the lowest.

allowing access to the temperature sensors and the dc heater which are thermally anchored to the back of the sample surface. The cylinder volume is sealed at the bottom end with a DN100 stainless steel flange [see Figs. 1(a) and 1(b)] and kept in a high vacuum for thermal insulation. Thanks to this configuration, the sample is efficiently cooled by conduction through its support, and its temperature can be locally varied and controlled within ± 0.1 mK, while the whole QPR cavity is immersed in superfluid helium kept at a regulated constant pressure of 20 mbar, equivalent to a helium boiling temperature of 1.85 K.

When the QPR is excited at its resonance modes, the rf currents circulating in the rods create an image current on the sample surface underneath [see Fig. 1(c)]. All the quadrupole modes (TE_{21}-like) up to 2 GHz are such that the rf fields exponentially decay down the 2 mm coaxial gap around the sample cylindrical support. This ensures that the power dissipation in the gap, and, in particular, at the normal conducting end flange and copper joint, is negligible. The QPR is equipped with three antennas to couple input rf power into it and to pick up transmitted power. The actual rf hardware is designed for probing from the fundamental quadrupole mode up to the third harmonic ($f_0 \approx 400$ MHz, $f_1 \approx 800$ MHz, and $f_2 \approx 1200$ MHz). For a more detailed description of the QPR and of its working principle, in particular, of the calorimetric testing technique for superconducting samples, we refer to Refs. [17,18], and references therein.

For this work, in which only normal conducting samples are characterized, an estimate of the surface resistance R_s is obtained from the measurement of the loaded quality factor Q_L of the whole QPR cavity. The loaded quality factor is measured in transmission by means of a vector network analyzer (VNA) as the ratio of the center frequency and the full width at half maximum of the resonance curve. When a cavity is coupled to the experimental setup for its test, Q_L is given by the combination of the internal (or unloaded) quality factor Q_0, which is a measurement of the internal losses per rf cycle, and of the external quality factor Q_{ext}, which takes into account the dissipation of the rf field towards the external environment. In the case of the QPR, the unloaded Q_0 is itself a combination of two terms: the losses from the host cavity Q_c and from the sample Q_s. The loaded Q_L thus is written as $Q_L^{-1} = Q_c^{-1} + Q_s^{-1} + Q_{ext}^{-1}$. As the QPR cavity is submerged in superfluid helium at a constant pressure of 20 mbar ($T \approx 1.85$ K) during the test, the bulk niobium is in the superconducting state, and, thus, the associated rf losses are several orders of magnitude lower than those of a normal metal such as copper. In this specific case, $Q_c \geq 10^9 \gg Q_s$; thus, Q_c can be disregarded and thence $Q_L^{-1} \approx Q_s^{-1} + Q_{ext}^{-1}$. The external Q_{ext} is instead fixed by the antenna design, and its value is of the order of 10^6. The exact values were measured during the characterization of a superconducting sample, for which $Q_c, Q_s \geq 10^9 \gg Q_{ext}$. To obtain the R_s value, we then use the definition of Q_s. The sample unloaded quality factor at frequency $f = \frac{\omega}{2\pi}$ is defined as

$$Q_s = \frac{\omega U}{P_s} = \frac{\omega \mu_0 \int_{V_s} |H|^2 dv}{\int_{\Gamma_s} R_s |H|^2 ds}, \qquad (1)$$

where U is the energy stored in the sample volume V_s, P_s is the rf power dissipated over the exposed sample surface Γ_s, and μ_0 is the magnetic permeability of the vacuum. Then, assuming a uniform surface resistance R_s over the investigated sample surface,[1] one has

$$R_s = G/Q_s, \qquad (2)$$

where

$$G \equiv \frac{\omega \mu_0 \int_{V_s} |H|^2 dv}{\int_{\Gamma_s} |H|^2 ds} \qquad (3)$$

is a coefficient referred to as the geometric factor, which is calculated for each mode via numerical simulations made by CST Studio Suite and/or ANSYS [19]. To ensure a good fidelity of the simulations results, an accurate knowledge of the QPR geometry is necessary. Moreover, as G depends on the distance between the sample top surface and the bottom of the QPR rods, an accurate measurement of the height of each sample support is also required. Slightly different G values have then been used to estimate R_s using Eq. (2), in order to take into account the measured differences in height.

B. Sample preparation

Two twin copper samples have been fabricated and used to study the different surface treatments of interest. The first one, referred to as Cu_A, was first measured for reference and then structured by laser irradiation. Two different patterns were followed when laser structuring the pristine copper: a radial and a circular one (see section "laser treatment" for more details), respectively labeled as LESS1 and LESS2. The second copper sample (Cu_B) was coated with a 260-nm-thick titanium sublayer and a 100-nm-thick amorphous carbon top layer (see Sec. II D for more details), after the reference measurement. An image of the four different surface conditions (pristine Cu, LESS1, LESS2, and a-C coating) is displayed in Fig. 2. The samples are manufactured from a flat disk of high-purity copper of RRR $\approx 100^2$ (UNS type C10100, often referred to as "OFE copper"), typical of accelerator components. This is joined

---

[1]In a more realistic scenario, R_s is not constant over the sample surface, and therefore Eq. (2) represents its average value.

[2]RRR (residual resistivity ratio) is the ratio of the electrical resistivities measured at room temperature and at 4.2 K (or just above the critical temperature, for superconductors) and is a typical measurement of metal purity. The ratio is insensitive to specimen geometry and can be calculated also as the ratio of electrical resistances; thus, it is useful to characterize irregular shapes.
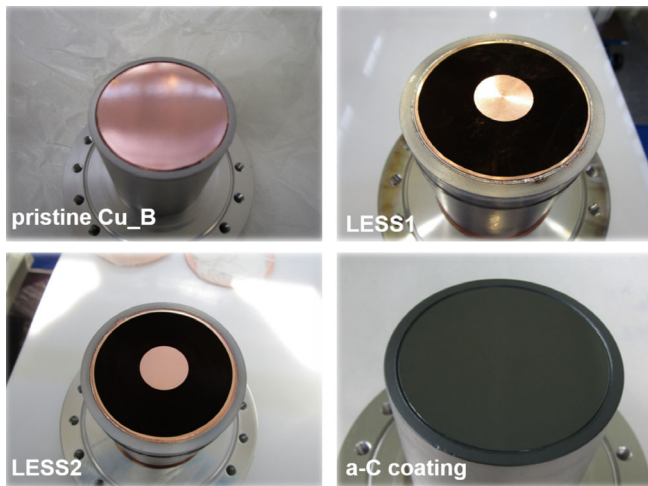
FIG. 2. The four characterized sample surfaces. Cu_A or Cu_B, pristine OFE copper; LESS1, copper with a radial laser pattern; LESS2, copper with a circular laser pattern; a-C coating, copper with an amorphous carbon coating.

to a high-purity RRR $\approx$ 300 bulk niobium ring by melting their interfaces by e-beam, reliably achieving a UHV tight seam. This is in turn e-beam welded to a bulk niobium cylinder (RRR $\approx$ 40) which was previously brazed to a 6" conflat stainless steel flange with a copper filler [see Fig. 2(b)]. All weldings are performed after a chemical etching of about 20 μm. The samples are then finished with a standard surface chemical polishing treatment for copper, removing about 150 μm. A similar surface treatment, limited to 60 μm, was performed also prior to LESS2, in order to erase the traces of LESS1.

Prior to the rf test, the surface of all samples except the a-C-coated one has been rinsed with ultrapure water at 3 bar in a clean room and kept in nitrogen atmosphere once dry, as is standard practice for superconducting rf test devices and components in order to remove any dust particles. The a-C-coated sample has instead only been blown with purified nanofiltered nitrogen, to avoid possible

degradations or peel-off of the film. It has been verified on witness samples that the rinsing does not substantially alter the surface of LESS, changing the maximum SEY of less than 0.1 units, as illustrated in Fig. 3(a). Details of the SEY measurement technique are discussed elsewhere [6]. The SEY of a typical Ti- or a-C-coated Cu sample is also shown for reference in Fig. 3(a).

C. Laser treatment

The laser surface structuring was carried out using a linearly polarized 10-ps pulsed laser with a wavelength of 532 nm at a repetition rate of 200 kHz. The laser beam had a Gaussian intensity profile ($M^2 < 1.3$) and was focused onto the surface using a telecentric lens that allowed for offsetting the off-axis deflection of the beam through the focusing lens system. The diameter of the focused spot—between the points where the intensity has fallen to $1/e^2$ of the central value—was measured to be $\sim$12 μm. Throughout the experiments, an average laser pulse energy of 5 μJ was used, leading to a laser energy fluence of approximately 4.2 $J\,cm^{-2}$ and a laser beam intensity of $\sim$0.4 $TW\,cm^{-2}$ in the focus for the required laser surface structuring. Using these laser beam parameters, a ring on the QPR samples with an outer diameter of 62 mm and an inner diameter of 22 mm, corresponding to the region where >99% of the rf power is dissipated [21], was filled with the required structures exhibiting low SEY. The structures were created using a line pattern with the distance between consecutive lines kept at approximately 24 μm. The surface was laser structured at the scanning speed of 10 mm/s, leading to approximately 240 pulses per spot being fired onto the target. All these values are equivalent to what was used for earlier accelerator validation experiments [12,20], to which the reader is referred for a detailed discussion of the laser parameter choices. A scanning electron microscope (SEM) image of a typical copper surface with LESS is shown in Fig. 3(b), where both the deep grooves created by the laser scanning and the fine
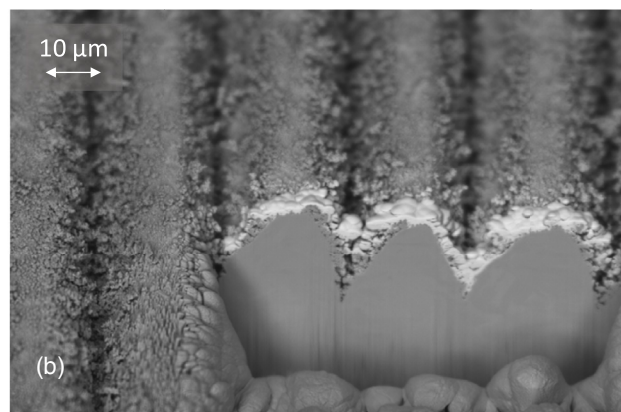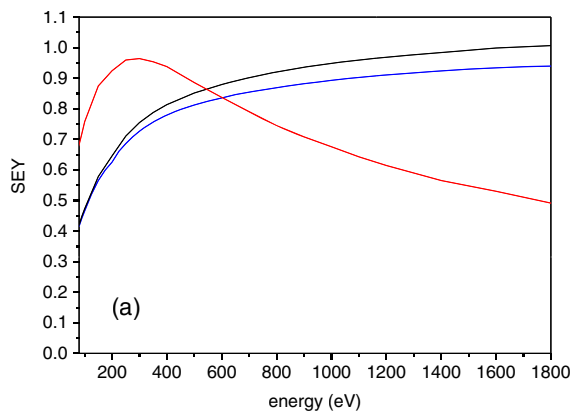

FIG. 3. (a) SEY measurement of LESS witness samples, before (blue line) and after water rinsing (black line), and of a typical a-C-coated Cu sample (red line). (b) SEM image of a cross section of a LESS sample (reproduced from Ref. [20] with STM permissions).
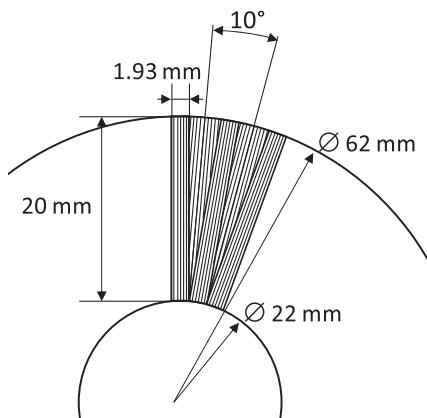
FIG. 4. Schematic pattern for the laser treatment of the QPR sample LESS1, repeated along the entire annular surface.

copper nanoparticles attached to the surface which result from the laser ablation process are clearly visible.

For sample LESS1, the lines were written nearly radially, in the pattern shown in Fig. 4. The ring was divided into rectangles of 20 mm height and 1.93 mm width, rotated 10° from one to the next. Each rectangle was filled with lines parallel to its long sides. The remaining triangles in between were also filled with lines, aligned with the bisector of the angle made by the neighboring rectangles. Hence, the angle of the lines filling the triangles had an angle of 5° relative to the lines filling the neighboring rectangles. This pattern guarantees that the rf currents cross orthogonally the lines etched by the laser beam within at most $\pm 5°$.

For sample LESS2, the laser and scanning parameters were kept identical, but the lines were etched in a single spiral pattern starting from the inner circle and covering the same annular dimensions as for sample LESS1.

Both treatments were carried out in air. After treatment, the samples have been stored in special enclosures avoiding any damage or impact to the surface. The time between the laser treatment and the rf measurement was of the order of several weeks. Previous experiments indicate that copper with LESS maintains a stable low SEY when stored in air up to one year [20].

D. Carbon coating

Given the tubular geometry of the beam screens of the HL-LHC magnets, the a-C coating is deployed using a short (~60 cm) cylindrical magnetron sputtering source with two independent targets (titanium and graphite) pulled

by cables along the beam screens (up to 20 m) [7]. In a first step, a titanium sublayer with a thickness of 100 nm is directly applied on the copper surface. The role of this titanium sublayer is to enhance the adhesion to the beam screen surface. In a second step, without intermediate exposure to the atmosphere, the a-C layer is deposited on top of the titanium. During the deposition of the carbon, titanium is also simultaneously deposited (and subsequently covered with the carbon as the sputtering source advances along the beam screen), in order to maintain a low partial pressure of hydrogen in the discharge gas via getter-pumping effect and ensure the low SEY of the a-C layer [6]. The chosen thicknesses are 250 nm for the titanium and 100 nm for the a-C films.

To adapt for the flat geometry of the QPR sample used in the present work, the titanium and the a-C layers were instead deposited using two planar magnetron sputtering sources with a diameter of 150 mm and an unbalanced magnetic assembly. The purities of the targets are 99.5% for the titanium and 99.92% for the graphite. The distance between the targets and the surface of the QPR sample was 135 mm. Before starting the coating, the system was baked at 135 °C for a duration of 46 hr, attaining a base pressure of 1×10^{-8} mbar after cooling down to room temperature. Argon (purity 99.9999%) was used as a discharge gas at a pressure of 7.4×10^{-4} mbar. First, a 260-nm-thick titanium layer was deposited followed by the growth of a 100-nm-thick a-C coating without intermediate exposure to air. The main coating parameters are listed in Table I.

After the coating process, the QPR sample was exposed to laboratory air and afterwards stored in a nitrogen atmosphere prior to the final filtered nitrogen blowing and assembly for the rf test.

III. RESULTS

The QPR allows for the measurement of the surface resistance R_s of flat samples as a function of the temperature, rf frequency, and power. In the following and for all the presented results, an input power of 10 dBm from the VNA was used to determine R_s from the measurement of the unloaded quality factor, as described above. A measurement uncertainty $\delta R_s / R_s \approx 10\%$ has been evaluated, including the systematic uncertainty on G.

In Fig. 5(a), we show the values of R_s as a function of the sample temperature, at $f_0 \approx 400$ MHz for all the surface treatments investigated. The estimates are for all the cases in the mΩ range, as expected for copper at these temperatures and frequencies [22]. The surface resistance is nearly

TABLE I. Coating parameters used for the production of the a-C coating and the titanium sublayer.

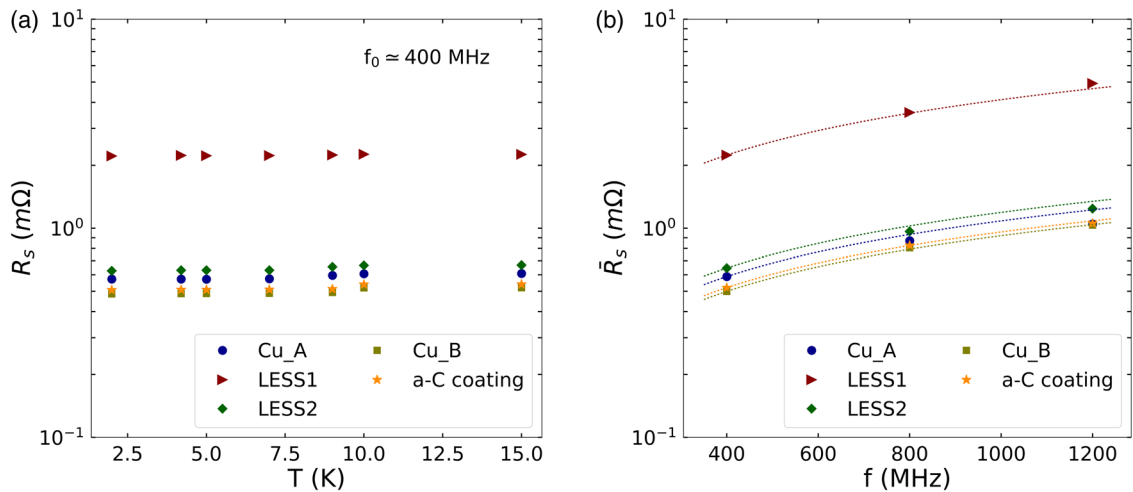| Layer	Ar pressure [mbar]	Power [W]	Voltage [V]	Current [mA]	Duration [min]	Thickness [nm]
Ti	7.4×10^{-4}	200	320	650	25	260
a-C	7.4×10^{-4}	400	740	540	25	100

FIG. 5.   (a) Surface resistance as a function of the sample temperature for pristine copper and for the different surface treatments. (b) Surface resistance averaged over the temperature as a function of the QPR mode frequency for pristine copper and for the different surface treatments. The curves show the functional dependence $f^{2/3}$, having the data points at 400 MHz as a reference. Error bars are not shown for a better visualization of the different data points (measurement uncertainty $\delta R_s / R_s \approx 10\%$).

constant in the range from 2 to 15 K, with a small increase starting from 10 K due to the contribution of the niobium parts surrounding the copper sample, gradually turning normal conducting when the sample temperature is increased above the superconducting critical temperature of 9.2 K.

On the other hand, an increase of the surface resistance is observed as a function of the QPR mode frequency, as displayed in Fig. 5(b). Here, $\bar{R}_s$ represents the average value over temperature for a given frequency.

Of great interest is, of course, the impact of the different treatments on the copper surface resistance. In Fig. 6, we plot the ratio of the surface resistance as a result of each treatment R_s^1 with respect to pristine copper R_s^0 versus both the temperature (a) and the frequency (b). Our findings

indicate that the three different studied cases have a finite impact on the R_s values. However, both the laser treatment with a spiral pattern (LESS2) and the a-C coating have a minor effect, with an R_s increase of only about 10% and 4%, respectively. On the other hand, the radial pattern (LESS1) with etched lines orthogonal to the rf currents results in an approximately 4–5 times larger R_s [triangles in Fig. 6]. The temperature dependence is nearly flat for all studied cases [see Fig. 6(a)], whereas we do observe a variation in the frequency [see Fig. 6(b)]. In the specific, the experimental data show an increment of the average $\bar{R}_s^1 / \bar{R}_s^0$ ratio as a function of the frequency for the two laser treatments. In the case of the a-C coating, instead, no variation is observed within the experimental uncertainty.
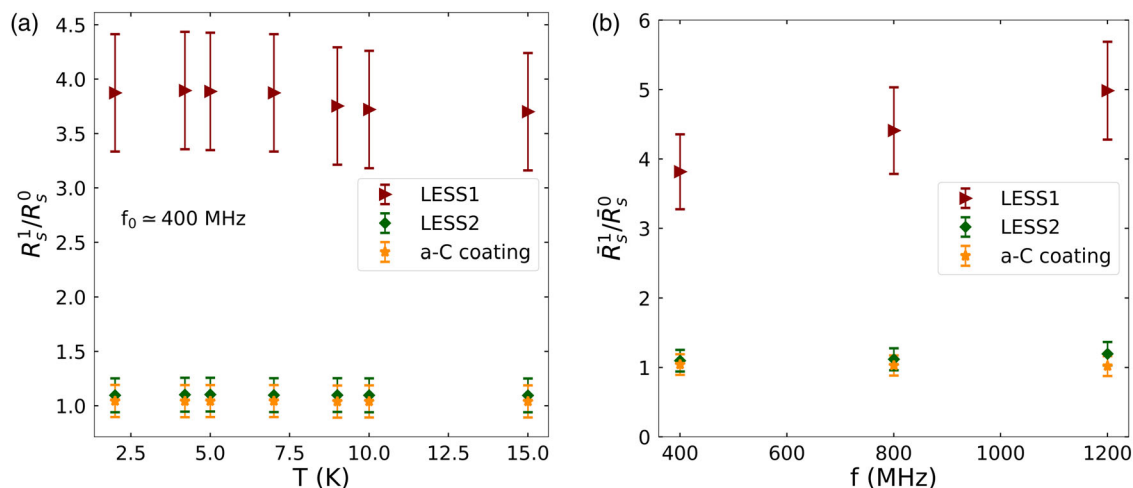

FIG. 6.   (a) Relative increase of the surface resistance with respect to pristine copper as a function of the temperature for the different surface treatments. (b) Relative increase of the average surface resistance with respect to pristine copper as a function of the frequency for the different surface treatments. Error bars are estimated from measurement uncertainty propagation.

IV. DISCUSSION

The results in Fig. 5(b) suggest that the copper surface is in the anomalous skin effect (ASE) regime, defined by the condition $l \gg \delta$ [23], where l is the electron mean free path and δ is the skin depth of the metal. In the extreme ASE regime, the scaling in frequency of $R_s \propto f^\alpha$ is with $\alpha = 2/3$, as illustrated in Fig. 5(b), instead of $\alpha = 1/2$, which is the typical power law of the normal skin effect in metals (when $l \ll \delta$). Our calculations[3] of the surface resistance taking into account the full ASE theory [23] and the temperature-dependent copper conductivity [24] indicate that the measurements are indeed in agreement with expectations for high-purity copper (RRR in the range 100–200). The good agreement further validates the experimental methods employed. More data points in frequency and temperature would be necessary for a deeper quantitative analysis, which goes beyond the scope of the present work.

The increase of $\bar{R}_s^1/\bar{R}_s^0$ with the frequency of sample LESS1 [see Fig. 6(b)] is likely due to the peculiar surface topography, illustrated in Fig. 3(b). Topography effects (see Refs. [26,27], and references therein) result in a behavior which strongly depends on the characteristic dimensions of the surface features, which we may call globally t, and their relationship with the skin depth, often resulting in an effective increase of the surface resistance at high frequencies, when $t \gg \delta$. In our case, δ can be estimated in the range 0.1–0.5 μm, depending on the frequency and on the RRR of copper. The grooves have a spacing of 24 μm and a depth of approximately 35 μm [20], both much larger than δ, while the fine copper nanoparticles attached to the surface have a size of the order of δ. Experimentally, we observe a large increase of the surface resistance for sample LESS1, where the surface currents are perpendicular to the grooves, and only a minor change for parallel currents, as is the case for sample LESS2. This particular behavior is indeed expected from the literature for grooves having dimensions $t \gg \delta$ where, without going into the details of the modeling [26,14], the longer path traveled by the surface currents when crossing the grooves perpendicularly may intuitively explain the phenomenon. We can obviously infer from this that the fine copper nanoparticles attached to the surface, being uniformly present in both configurations, are not at the origin of the difference between the two samples. For the same reason, we can exclude that the difference in surface resistance is due to a major change of electrical resistivity in LESS-treated samples, as would be the case for a homogenously increased impurity or defect content. This would, moreover, result in a regime closer to the normal skin effect and, thus, an exponent $\alpha = 1/2$ as

discussed previously, resulting in a decrease of $\bar{R}_s^1/\bar{R}_s^0$ with the frequency.

We cannot conclude from the measurements what is the origin of the minor increase of surface resistance still observed for sample LESS2, of the order of 10% relative to the reference copper, and several hypotheses could be suggested. The surface currents are not perfectly circular on the samples, in particular, near the split between the pedestals of the rods of the QPR. Considering the radial and the azimuthal current components separately, the power dissipated by the former on a plain copper surface would be roughly 1% of the total; thus, the radial component might indeed result in a small increase of surface resistance for sample LESS2 (it might also have the opposite effect on sample LESS1, being parallel to its radial grooves). The measured increase might also be due to a slight topography effect of the fine attached copper particles, which are present in equal amounts on both tested samples and have a size of the order of δ. Finally, it could be generated by some minor contamination, and RRR measurements performed on *ad hoc* 75-μm-thick copper samples, showing a decrease of RRR from about 70 to 35 after LESS treatment, would partly support this hypothesis. Any such phenomenon would nevertheless have an effect also on the surface resistance of radial grooves, albeit overshadowed by the much stronger effect of the path of the surface currents described earlier.

In the case of the a-C coating, no change of the surface resistance is observed within the experimental uncertainty, neither in absolute nor in relative terms compared to copper. This is consistent with calculations[3] which show that a very resistive thin film having a thickness $d \ll \delta$ (δ being the skin depth of the a-C or Ti material in this case), adds a negligible contribution to the surface resistance of the high-RRR copper underneath, estimated to less than 1% for the double layer a-C/Ti. Such surface coating would then not induce any significant increase of the wake losses compared to copper in the HL-LHC and allow consistently an SEY < 1, thus confirming the validity of this choice as the baseline for e-cloud suppression and justifying the development of an *in situ* sputter coating system as described above.

In situ deployment of LESS in the HL-LHC beam screens could be envisaged, on the other hand, by means of a robotized scanning system connected to the laser via an optical fiber. The proposed robot [10] would advance in the beam screen while its rotating head would etch lines spiraling around the beam screen circumference. The beam image current would thus flow perpendicularly to the grooves, as for sample LESS1 and as was also the case in the mentioned COLDEX experiment [12]. Such a pattern would then bring a considerable increase of the heat load due to rf heating from wake losses, about 4–5 times compared to copper at 20 K, based on our experimental data. In the case of the interaction region 8 (IR8) of the

---

[3]Original *Mathematica* (Wolfram Inc.) scripts based on Refs. [23,24] for ASE and on Ref. [25] for double layers.

HL-LHC, for example, it can be estimated that the power from wake losses would increase up to about 65 W [4]. Since the SEY of LESS is consistently <1, the e-cloud would nevertheless be totally suppressed, and a negligible power deposition onto the beam screen would ensue, largely compensating the increase of the wake losses. We should, however, point out that the estimated ultimate local cryogenic capacity is of the order of 195 W [7]; thus, in the case of a suboptimal treatment, even an SEY as low as 1.1 would result in an e-cloud power of about 120 W, bringing the total power close to the allowed limit [4]. The power deposited by collision debris would add to this balance; thus, a treatment system allowing for grooves parallel to the beam image current would ensure a larger margin.

V. CONCLUSIONS AND OUTLOOK

The surface resistance at cryogenic temperatures of different LESS treatments and of a-C coatings on copper has been measured using the quadrupole resonator, in a frequency range of relevance for studying wake-induced losses in the HL-LHC. Coatings of a-C, as expected due to their high resistivity and very low thickness compared to the skin depth, have a negligible impact on the surface resistance, and thus their choice as a baseline treatment for the HL-LHC is fully justified. The impact of LESS depends instead greatly on the relative orientation between the rf surface currents and the grooves inscribed by the laser during the surface structuring. When the grooves are parallel to the current, the impact on the surface resistance is also minimal. A perpendicular orientation results in an increase of the surface resistance of a factor of 4–5, in the frequency range explored. For an application in the existing interaction regions of the HL-LHC, the gain in power reduction due to e-cloud suppression would nevertheless outweigh the increase of power dissipation due to wake losses, even for a perpendicular orientation, as is envisaged in the current studies. However, implementation on a larger scale than only in the interaction regions would certainly call for a minimization of the contribution to the machine impedance and to the overall power consumption; thus, a treatment system capable to engrave a parallel pattern should be envisaged.

ACKNOWLEDGMENTS

[1] F. Zimmermann, Review of single bunch instabilities driven by an electron cloud, Phys. Rev. ST Accel. Beams **7**, 124801 (2004).

[2] M. Tobiyama, J. W. Flanagan, H. Fukuma, S. Kurokawa, K. Ohmi, and S. S. Win, Coupled bunch instability caused by an electron cloud, Phys. Rev. ST Accel. Beams **9**, 012801 (2006).

[3] F. Zimmermann, Electron cloud effects in the LHC, in *Proceedings of the Mini Workshop on Electron Cloud Simulations for Proton and Positron Beams, CERN, Geneva, 2002* (CERN, Geneva, 2002), pp. 47–55 (Report No. CERN-2002-001), http://dx.doi.org/10.5170/CERN-2002-001.47.

[4] G. Skripka and G. Iadarola, Beam-induced heat loads on the beam screens of the inner triplets for the HL-LHC, Report No. CERN-ACC-NOTE-2018-0009, http://dx.doi.org/10.17181/CERN.I7WJ.TNS9.

[5] G. Iadarola, E. Metral, and G. Rumolo, Beam induced heat loads on the beam-screens of the twin-bore magnets in the IRs of the HL-LHC, CERN Internal Note No. CERN-ACC-2016-0112, http://dx.doi.org/10.17181/CERN.ENUJ.1L15.

[6] P. Costa Pinto, S. Calatroni, H. Neupert, D. Letant-Delrieux, P. Edwards, P. Chiggiato, M. Taborelli, W. Vollenberg, C. Yin-Vallgren, J. L. Colaux, and S. Lucas, Carbon coatings with low secondary electron yield, Vacuum **98**, 29 (2013).

[7] P. Chiggiato, Beam screen coating, in *Proceedings of the LHC Performance Workshop, Chamonix 2018*, edited by F. Bordry, B. Delille, and M. Zerlauth (CERN, Geneva, 2018), https://indico.cern.ch/event/676124/contributions/2775544/.

[8] G. Tang, A. C. Hourd, and A. Abdolvand, Nanosecond pulsed laser blackening of copper, Appl. Phys. Lett. **101**, 231902 (2012).

[9] R. Valizadeh, O. B. Malyshev, S. Wang, S. A. Zolotovskaya, W. A. Gillespie, and A. Abdolvand, Low secondary electron yield engineered surface for electron cloud mitigation, Appl. Phys. Lett. **105**, 231605 (2014).

[10] M. Sitko, V. Baglin, S. Calatroni, P. Chiggiato, B. Di Girolamo, E. Garcia-Tabares Valdivieso, M. Taborelli, M. Colling, T. Jones, P. McIntosh, D. Bajek, S. Wackerow, and A. Abdolvand, Towards implementation of laser engineered surface structures for electron cloud mitigation, in *Proceedings of the Ninth International Particle Accelerator Conference (IPAC'18), Vancouver, 2018* (JACoW, Geneva, 2018), pp. 1220–1223, https://doi.org/10.18429/JACoW-IPAC2018-TUZGBE3.

[11] R. Salemme, V. Baglin, G. Bregliozzi, P. Chiggiato, and R. Kersevan, Amorphous carbon coatings at cryogenic temperatures with LHC type beams: First results with the COLDEX experiment, in *Proceedings of the Sixth International Particle Accelerator Conf. (IPAC'15), Richmond, VA, 2015* (JACoW, Geneva, 2015), pp. 3112–3114, https://doi.org/10.18429/JACoW-IPAC2015-WEPHA007.

[12] R. Salemme, V. Baglin, S. Calatroni, P. Chiggiato, B. Di Girolamo, E. Garcia-Tabares Valdivieso, B. Jenninger, L. Prever-Loiri, M. Sitko, S. Wackerow, and A. Abdolvand, First beam test of laser engineered surface structures

(LESS) at cryogenic temperature in CERN SPS accelerator, J. Phys. Conf. Ser. **1067**, 082017 (2018).

[13] N. F. Mounet, HL LHC: Impedance considerations for the new triplet layout in IR1 & 5, in https://indico.cern.ch/event/259525/.

[14] O. E. Berrig, Update of impedance of LESS surface treatment, in https://indico.cern.ch/event/524108/timetable/.

[15] R. Valizadeh, O. B. Malyshev, S. Wang, T. Sian, L. Gurran, P. Goudket, M. D. Cropper, and N. Sykes, Low secondary electron yield of laser treated surfaces of copper, aluminium and stainless steel, in *Proceedings of the Seventh International Particle Accelerator Conference (IPAC'16), Busan, Korea, 2016* (JACoW, Geneva, 2016), TUOCB02, pp. 1089–1092, ISBN: 978-3-95450-147-2, https://doi.org/10.18429/JACoW-IPAC2016-TUOCB02.

[16] E. Métral, rf heating from wake losses in diagnostics structures, in *Proceedings of the International Beam Instrumentation Conference, Oxford, 2013*, edited by I. Martin and G. Rehm (JACoW, Geneva, 2013), p. 929, http://accelconf.web.cern.ch/AccelConf/IBIC2013/papers/thbl1.pdf.

[17] E. Mahner, S. Calatroni, E. Chiaveri, E. Haebel, and J. M. Tessier, A new instrument to measure the surface resistance of superconducting samples at 400 MHz, Rev. Sci. Instrum. **74**, 3390 (2003).

[18] T. Junginger, W. Weingarten, and C. Welsch, Extension of the measurement capabilities of the quadrupole resonator, Rev. Sci. Instrum. **83**, 063902 (2012).

[19] T. Junginger, Investigation of the surface resistance of superconducting materials, Ph.D. thesis, Heidelberg University, 2012, https://cds.cern.ch/record/1489972.

[20] S. Calatroni, E. Garcia-Tabares Valdivieso, H. Neupert, V. Nistor, A. T. Perez Fontenla, M. Taborelli, P. Chiggiato, O. Malyshev, R. Valizadeh, S. Wackerow, S. A. Zolotovskaya, W. A. Gillespie, and A. Abdolvand, First accelerator test of vacuum components with laser-engineered surfaces for electron-cloud mitigation, Phys. Rev. Accel. Beams **20**, 113201 (2017).

[21] V. Del Pozo Romano (private communication).

[22] J. T. Rogers, S. De Panfilis, A. C. Melissinos, B. E. Moskowitz, Y. K. Semertzidis, W. U. Wuensch, H. J. Halama, A. G. Prodell, W. B. Fowler, and F. A. Nezrick, Anomalous rf magnetoresistance in copper at 4 K, Appl. Phys. Lett. **52**, 2266 (1988).

[23] G. E. H. Reuter and E. H. Sondheimer, The theory of the anomalous skin effect in metals, Proc. R. Soc. A **195**, 336 (1948).

[24] N. J. Simon, E. S. Drexler, and R. P. Reed, Properties of Copper and Copper Alloys at Cryogenic Temperature, *NIST Monograph* 177 (NIST, Boulder, 1992), https://doi.org/10.6028/NIST.MONO.177.

[25] J. A. Stratton, *Electromagnetic Theory* (McGraw-Hill, New York, 1941), p. 511.

[26] S. P. Morgan, Effect of surface roughness on eddy current losses at microwave frequencies, J. Appl. Phys. **20**, 352 (1949).

[27] K. Lomakin, G. Gold, and K. Helmreich, Analytical waveguide model precisely predicting loss and delay including surface roughness, IEEE Trans. Microwave Theory Tech. **66**, 2649 (2018).